Behavior of Si Photoelectrodes under High Level Injection Conditions. 2. Experimental Measurements and Digital Simulations of the Behavior of Quasi-Fermi Levels under Illumination and Applied Bias

Olaf Krüger, C. N. Kenyon, Ming X. Tan, and Nathan S. Lewis*

Division of Chemistry and Chemical Engineering, California Institute of Technology, Pasadena, California 91125

Received: August 14, 1996; In Final Form: December 3, 1996[⊗]

Use of thin, nearly intrinsically doped Si electrodes having implanted, interdigitated n^+ and p^+ back contact points has allowed electrical control over the potential of either electrons or holes in the solid. During potential control at the n^+ point contacts, the open-circuit potential of holes could be monitored, while during potential control of the p^+ point contacts, the open-circuit potential of electrons was measured. In combination with current density−voltage measurements of either electrons or holes passing through the back contact points, these data allowed a comparison of the behavior of a given carrier type when generated by an applied bias (i.e., as majority carriers) relative to their behavior when generated with band gap illumination of the solid (as minority carriers). Data have been collected for Si/CH_3OH junctions having 1,1′-dimethylferrocene$^{+/0}$, decamethylferrocene$^{+/0}$, methyl viologen$^{2+/+}$, and cobaltocene$^{+/0}$ as redox couples. These data have been used to validate certain key predictions of the quasi-Fermi level concept in photoelectrochemistry. In addition, digital simulations that include two-dimensional representations of the charge density distribution and of the current fluxes in the solid have been utilized to provide a quantitative understanding of the observed experimental behavior.

I. Introduction

The preceding paper describes the current density vs voltage ($J-V$) behavior of Si photoelectrodes under high level injection conditions and also presents a theoretical and experimental analysis of the factors that control the photovoltage and the photocurrent directionality of such samples.[1] As discussed in that paper, these experiments have provided insight into the open-circuit behavior of the quasi-Fermi levels of semiconductor/liquid contacts. The measurements have also led to a kinetic description of the photocurrent and photovoltage behavior of such systems.

The electrical junction configuration fabricated into these samples also offers the possibility of controlling electrically the potential at, and measuring the charge carrier flux through, one collection of contacts while monitoring the electrochemical potential (at open circuit) produced at the other set of contacts. Such measurements, described herein, allow investigation of the position of the quasi-Fermi level for a given carrier type in the presence of band gap excitation of the semiconductor, under a variety of bias conditions and for a variety of redox couples in the liquid phase. These results are relevant to the controversy regarding the thermodynamic interpretation of the quasi-Fermi levels in an operating, illuminated photoelectrochemical cell and are of fundamental interest with respect to the behavior of the quasi-Fermi levels under an applied bias.[2−9] This paper describes experimental data and digital simulations of the carrier generation, transport, and recombination processes in such systems. The simulations have been performed to confirm quantitatively some of the approximations advanced in the preceding and present papers[1,10−12] and to provide insight into some unexpected aspects of the behavior of quasi-Fermi levels that have been observed during the course of this study.

II. Methods and Procedures

All samples, experimental methods, and measurement protocols were described in the preceding paper.[1] Numerical device simulations were performed using the Two-dimensional Semi-Conductor Analysis (ToSCA) software package. ToSCA was developed by Gajewski and co-workers for numerical simulation of carrier transport in semiconductors.[13] The code is based upon van Roosbroeck's drift-diffusion model,[14] which consists of a differential equation system that includes Poisson's equation and the continuity equations for electrons and holes. ToSCA solves this system of equations numerically and self-consistently calculates the potential distribution and concentration profiles of charge carriers in the solid in accord with Fermi−Dirac statistics. Optical generation of carriers, as well as bulk and surface recombination, are incorporated explicitly into the ToSCA package. The simulation of specific electrical contacts (e.g., gate or ohmic) is accomplished by the imposition of suitable boundary conditions. A more detailed description of the mathematical and physical models used in ToSCA can be found in a previous publication and references therein.[15]

The interface between the semiconductor and the electrolyte was modeled by modifying the boundary conditions initially incorporated into the ToSCA package. The ToSCA boundary conditions representing a solid-state gate oxide contact were changed to reflect the physical properties of the Helmholtz double layer. Specifically, the gate was specified to be a leaky dielectric having a thickness of 0.3 nm and a dielectric constant of $6\epsilon_0$ (as expected for directed water dipoles[16]) where ϵ_0 is the permittivity of free space. Charge transfer across this gate oxide represented the faradaic current flow due to oxidation or reduction of the redox species in the electrolyte. Band edge shifts were computed self-consistently as a result of any change in surface charge produced across this dielectric layer.

Marcus−Gerischer theory, as specified by eqs 1 and 2,[17−21] was used to calculate the interfacial charge-transfer current densities across the modified gate contact.[22]

* To whom correspondence should be addressed.
[⊗] Abstract published in *Advance ACS Abstracts,* February 1, 1997.

S1089-5647(96)02484-4 CCC: $14.00

$$j_c = -qk_c^{max} N_c c_{red} \exp\left[-\frac{(\mathbf{E}_c - \mathbf{E}^{o'}_{redox} + \lambda)^2}{4kT\lambda}\right]\left(\frac{n_s}{n_{so}} - 1\right) \quad (1)$$

$$j_v = qk_v^{max} N_v c_{ox} \exp\left[-\frac{(\mathbf{E}_v - \mathbf{E}^{o'}_{redox} - \lambda)^2}{4kT\lambda}\right]\left(\frac{p_s}{p_{so}} - 1\right) \quad (2)$$

In these expressions, q denotes the elementary charge, k denotes the Boltzmann constant, T denotes the temperature, $\mathbf{E}_c$ and $\mathbf{E}_v$ denote the energies of the conduction band and valence band of the semiconductor, respectively, N_c and N_v are the effective densities of states in the conduction band and the valence band, respectively, n_s is the surface electron concentration (having an equilibrium value n_{so}), p_s is the surface hole concentration (having a value at equilibrium of p_{so}), and k_c^{max} and k_v^{max} (having units of $cm^4\ s^{-1}$)[23−25] are the charge-transfer rate constants at optimal exoergicity for the conduction band and valence band processes, respectively. In these rate constant expressions, the concentrations of the redox species (c_{red}, c_{ox}) are multiplied by an exponential term, the so-called nuclear (or Franck−Condon) factor, that accounts for the fluctuation of the solvation shell around a redox species having a formal electrochemical potential $\mathbf{E}^{o'}_{redox}$ and a reorganization energy λ. Within the Gerischer formalism of semiconductor electrochemistry, this Franck−Condon term yields a measure of the overlap of occupied/empty states of the redox system with the states of the valence/conduction band of the solid.[26−29] The contribution of the semiconductor to the overall rate of charge transfer is determined by the effective density of states in the energy bands (N_c, N_v) and by the ratios of the carrier concentrations at the surface (n_s, p_s) to the interfacial carrier concentrations present under equilibrium conditions (n_{so}, p_{so}). The equilibrium carrier concentrations are determined by the barrier height of the semiconductor/liquid contact, which was known experimentally for the systems under study.[25,30−36] Thus, two parameters, k_{ct}^{max} ($k_c^{max} = k_v^{max}$ was always used in the simulations) and λ, were used to describe the exchange current densities resulting from charge transfer from the conduction and valence bands. While it is possible to infer the homogeneous reorganization energy of these ions from NMR measurements of self-exchange rate constants,[37] no experimental data for the reorganization energy of ions at the semiconductor/electrolyte interface appear to have been published.[36,38,39] Theoretical studies have suggested that λ for the oxidation/reduction of an outer-sphere redox species at a metal electrode is approximately one-half that for the same ion in a homogeneous self-exchange process.[40,41] However, the reorganization energy for a semiconductor/liquid system is predicted to be approximately twice that of the corresponding value at a metal/liquid interface, when only static dielectric contributions to the reorganization energy are included.[41,42] Due to these uncertainties, the reorganization energy for all of the redox couples used in this study was approximated as 0.5 eV.[35,36,43−48] A drawback to the ToSCA code as presently formulated is the inability to account for concentration polarization and series resistance losses in the electrolyte. Thus, the assumed interfacial charge-transfer rates were independent of time for given carrier concentrations in the solid, when in actuality, the experimental interfacial charge-transfer rates change with stirring rate, time, etc., to reflect the changes during current flow in the steady-state concentration of donor and acceptor species in the region of the electrolyte adjacent to the electrode surface.

The simulated electrode had $x-y-z$ dimensions of 120 × 60 × 10 μm (with the 120 μm dimension corresponding to the sample thickness and the 60 μm dimension corresponding to the width of the exposed electrode). Simulations were performed for the x and y directions, and the carrier concentrations were assumed to be uniform in the other dimension (z), which was parallel to the electrode surface.

Two-dimensional simulations were carried out in which the back had both n^+ and p^+ contacts, as in the actual sample (Figure 1 in the preceding paper). The two degenerately doped regions were specified in the simulation to be separated by 20 μm and to have individual dimensions of 10 μm in the y direction. The dopant profiles for these ohmic-selective contacts were generated by specifying the presence of high dopant concentrations at the back contact. The highly doped regions were specified to have dopant concentrations of 10^{18} cm^{-3} that were uniform over an x range of 1 μm (from the back of the sample) and then were allowed to decay into the bulk with a Gaussian distribution that reached 1/e of its maximum value in 8 μm. The background donor density was fixed throughout the bulk of the sample at the experimentally measured value of 3 × 10^{13} cm^{-3}, as determined from a four-point probe measurement of the sample resistivity. Figure 1a−c shows the potential distribution, as well as the carrier concentration profiles at equilibrium (in the dark), that result from these doping profiles for a Si/CH_3OH contact which has a barrier height of 0.6 V.

For comparison to experimental data, a series of simulations were performed using this two-dimensional back contact geometry in which the electron quasi-Fermi level was controlled through the n^+ ohmic contact and the hole quasi-Fermi level ($qV_{p+,oc}$) was calculated at the edge of the p^+ ohmic contact. For numerical reasons, ToSCA requires the current density through the p^+ contacts, J_{p+}, to be nonzero, so the open-circuit condition at the p^+ contacts under such conditions was modeled by specifying that $|J_{p+}| \leq 10$ nA cm^{-2}. In another series of simulations, the hole quasi-Fermi level was controlled through the p^+ ohmic contact, and the electron quasi-Fermi level was calculated at the edge of the n^+ ohmic contact. Under these conditions, the simulation was constrained so that $|J_{n+}| \leq 10$ nA cm^{-2}, where J_{n+} is the current density through the n^+ points.

Some aspects of the experimentally observed behaviors were modeled by simulations in which the back contact geometry was simplified to be uniformly degenerately doped with either electrons or holes. In these simulations, an n^+ region (of donor density, N_d, equal to 10^{18} cm^{-3}) was created at the back surface of the electrode for simulation of experiments in which the electron quasi-Fermi level was being controlled potentiostatically, while a p^+ region (of acceptor density, N_a, equal to 10^{18} cm^{-3}) was generated to simulate experiments in which the hole quasi-Fermi level was maintained under potentiostatic control. When this procedure was used, the experimentally measured quasi-Fermi level value for the carrier being monitored at open circuit was estimated as the simulated quasi-Fermi level value at the edge of the diffused back contacts ($x \approx 80-100$ μm from the solid/liquid contact). In other words, when the potential was being controlled at the n^+ points, the hole quasi-Fermi level that would be measured at the p^+ points was taken to be the value of the hole quasi-Fermi level computed at the edge of a spatially uniform, diffused n^+ back contact region. The simplified and full two-dimensional simulations were compared in several representative cases, and in each instance, the quasi-Fermi level positions calculated from the simplified sample were found to be virtually identical with those obtained from the simulations that contained the actual spatial distribution of the back point contacts.

Except for the charge-transfer rate constants, essentially all of the input parameters (Table 1) used in the digital simulation program were determined experimentally or were known from the literature. The bulk low-level minority carrier lifetime of

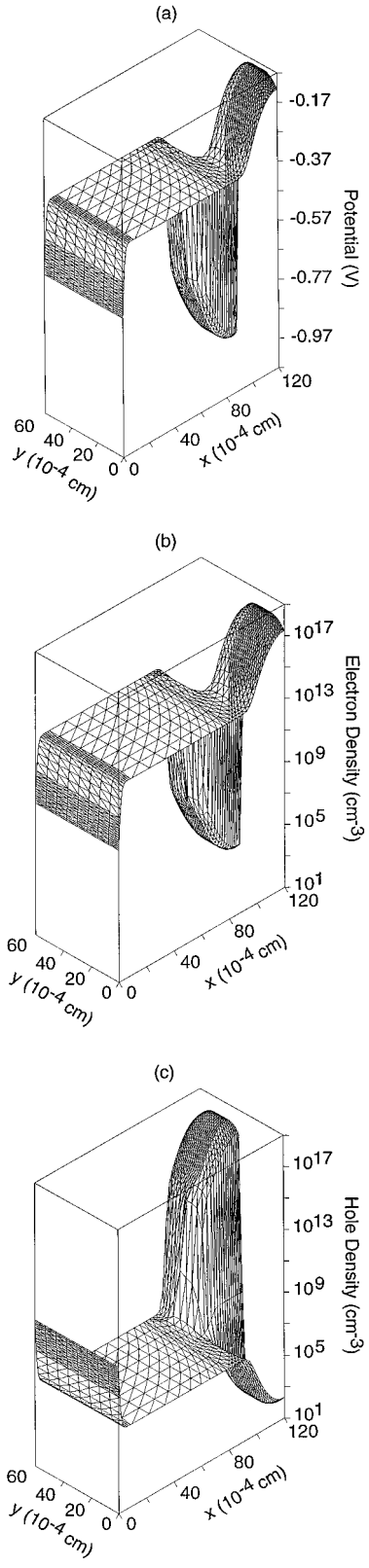

Figure 1. Results of the two-dimensional computer simulation of the initial condition in the dark (equilibrium) for an n-Si/liquid contact. The figures show the contact to the electrolyte at the left (front) side. The asymmetric back contact is situated at the right side of the figures. The Fermi level was set to be equal to the electrochemical potential of the solution, which was chosen to be zero. The rate constants for the electron and hole transfer were assumed to be equal, with $k_{ct}^{max} = 10^{-18}$ cm^4 s^{-1}. The concentrations were c_{red} =14 mM and c_{ox} = 17 mM, and the barrier height of the contact was 0.6 V. (a) Profile of the electric potential,[62] (b) profile of the electron concentration, and (c) profile of the hole concentration for this sample.

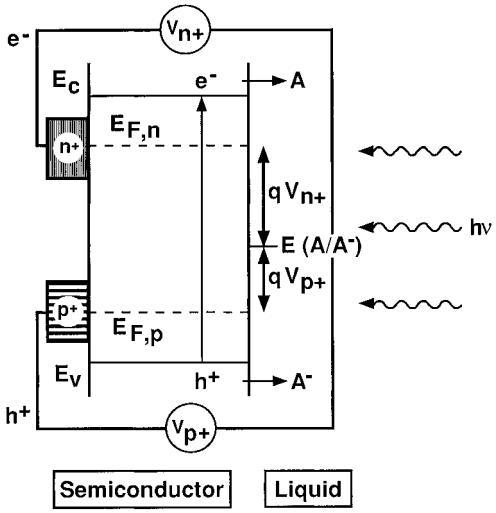

Figure 2. Schematic representation of the band diagram of the high purity Si/liquid junction under high level injection conditions. $\mathbf{E}_c$ and $\mathbf{E}_v$ represent the energies of the conduction band edge and valence band edge of the semiconductor, respectively. qV_{n+} is the energy difference measured between the n^+ point contacts and the solution electrochemical potential, $\mathbf{E}(A/A^-)$, while qV_{p+} is the energy difference measured between the p^+ point contacts and $\mathbf{E}(A/A^-)$. The voltages at the n^+ and p^+ contact points directly reflect the quasi-Fermi level positions of electrons and holes at the back of the sample, $\mathbf{E}_{F,n}(d) = qV_{n+}$ and $\mathbf{E}_{F,p}(d) = qV_{p+}$.

TABLE 1: Physical Input Parameters of the ToSCA Simulations

physical parameter	value	ref
intrinsic carrier concentration	$n_i = 1.45 \times 10^{10}$ cm^{-3}	56
dielectric constant	$\epsilon/\epsilon_0 = 11.9$	56
energy gap	$\mathbf{E}_g = 1.12$ eV	56
effective density of states in conduction band	$N_c = 2.8 \times 10^{19}$ cm^{-3}	56
effective density of states in valence band	$N_v = 1.04 \times 10^{19}$ cm^{-3}	56
electron mobility	$\mu_n = 1500$ cm^2 V^{-1} s^{-1}	56
hole mobility	$\mu_p = 450$ cm^2 V^{-1} s^{-1}	56
nonradiative bulk lifetime	$\tau_n = \tau_p = 1$ ms	49
coefficient of radiative recombination	$B = 6 \times 10^{-14}$ cm^3 s^{-1}	57
coefficient of Auger recombination	$C_n = C_p = 2 \times 10^{-31}$ cm^6 s^{-1}	58−61
absorption coefficient	$\alpha = 1.2 \times 10^4$ cm^{-1}	
reorganization energy	$\lambda = 0.5$ eV	35, 36, 43−48

these Si samples was 1 ms, and this was represented in the simulation by setting the nonradiative (Shockley−Read−Hall) bulk lifetime $\tau_n = \tau_p = 1$ ms.[49] The front surface recombination velocity, describing recombination mediated by surface states, was chosen to be 100 cm s^{-1}, which corresponds to the experimentally measured value for these Si/CH_3OH contacts.[10,12,50,51] Other specific input parameters for the simulations of this work are provided in the appropriate sections of the paper.

III. Results and Discussion

A. Experimental Measurement of Quasi-Fermi Level Characteristics at Si/Liquid Interfaces under Applied Bias. As depicted in Figure 2, the contact geometry in these samples provided an opportunity to set the potential of one carrier type in the photoelectrode while monitoring the potential adopted by the other carrier type. For example, the potential at the n^+ points could be controlled using a potentiostat (with $V_{n+} = E(n^+) - E(A/A^-)$ where $E(A/A^-)$ is the redox potential of the solution), while the current density for electron collection (J_{n^+}),

and the open-circuit potential of the p^+ points, $V_{p+,oc} = E(p^+) - E(A/A^-)$, were monitored. This type of experiment could be performed while the sample was under an arbitrary degree of illumination.

As a specific example, we refer first to electron collection, which was accomplished through potentiostatic control of the n^+ points. The current density vs voltage data for electron collection at these points, J_{n+} vs V_{n+}, have been presented as Figure 2 in the preceding paper. Figure 3a presents additional data for the $Si/CH_3OH-Me_2Fc^{+/0}$ contact in which the potential of the holes, $V_{p+,oc}$, was measured as a function of the potential applied to the n^+ points, V_{n+}. Such data were recorded independently of, but simultaneously with, measurements of the electron flux through the n^+ points at various values of V_{n+}. The sample was under illumination in this experiment in order to create a significant concentration of holes in the semiconductor.

There were two distinct regions of such plots. In the rising portion of the J_{n+} vs V_{n+} plot, where the current density at the n^+ points depended on the applied bias to the system, $V_{p+,oc}$ was observed to be a function of the potentiostatically controlled voltage V_{n+}. In the region where J_{n+} was independent of V_{n+}, no change in $V_{p+,oc}$ was observed, even for significant variation of V_{n+}. Thus, in this region, the difference between $V_{p+,oc}$ and V_{n+} was linearly dependent on the value of V_{n+}, with more positive V_{n+} values producing smaller separations of the electron and hole quasi-Fermi levels at the back of the sample. Although not shown in the figure, a third region of behavior, in which $V_{p+,oc}$ again became dependent on V_{n+}, was observed at sufficiently positive biases.

$V_{p+,oc}$ vs V_{n+} data for the other two redox couples that displayed significant photovoltages in this contact configuration are presented in Figure 3b,c. Two distinct regimes were observed for all such data. As described above for $Si/CH_3OH-Me_2Fc^{+/0}$ contacts, when the J_{n+} vs V_{n+} data exhibited a dependence on applied potential, changes in the potential applied to one contact produced changes in the open-circuit potential measured at the other contact. In the other regime, where the photocurrent density was limited either by mass transport or by the electron−hole pair generation rate, changing the voltage applied at the n^+ contact did not produce any changes in the open-circuit potential measured at the p^+ contact. In this regime of behavior, the quasi-Fermi level separation became smaller as the sample was driven further into reverse bias. As was observed for the $Si/CH_3OH-Me_2Fc^{+/0}$ system, $V_{p+,oc}$ was found to again become dependent on the value of V_{n+} at strong reverse bias (not shown in figures).

As shown in Figure 3d, the $Si/CH_3OH-CoCp_2^{+/0}$ system exhibited ohmic behavior in this experiment. This behavior is expected theoretically since the electrochemical potential of the $CoCp_2^{+/0}$ system is close to the conduction band edge energy of the semiconductor.[52]

It was also possible to measure, for this same series of semiconductor/liquid contacts under identical illumination conditions, the current−voltage properties of holes while monitoring the quasi-Fermi level behavior of electrons. These data were obtained by applying a bias to the p^+ points and measuring J_{p+} as well as $V_{n+,oc}$. Figure 4a displays the J_{p+} vs V_{p+} data for the $Si/CH_3OH-Me_2Fc^{+/0}$ contact, showing that this system exhibited near-ohmic behavior under illumination. As was the case for the $CoCp_2^{+/0}$ system when the n^+ points were controlled potentiostatically, the behavior of the $Si/CH_3OH-Me_2Fc^{+/0}$ contact under control of the p^+ points is expected since the electrochemical potential of the redox couple is close to the energy of the valence band edge.[36] Figure 4b−d displays

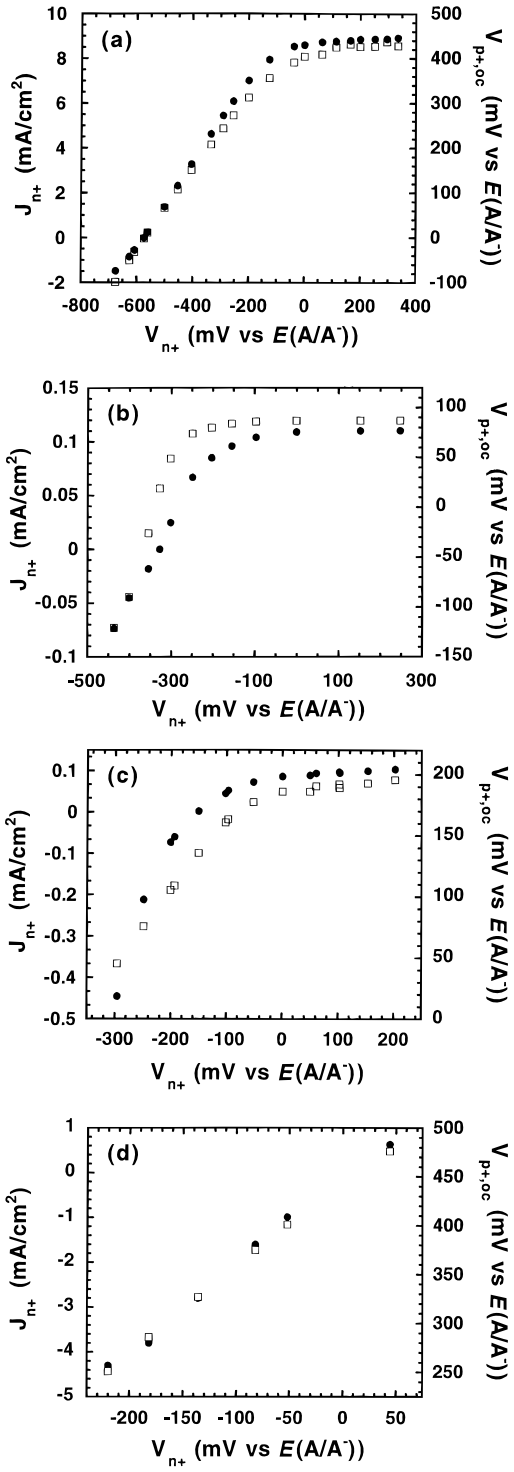

Figure 3. Plot of the open-circuit potential measured at the p^+ points ($V_{p+,oc}$, open squares) and current collected at the n^+ points (J_{n+}, solid circles) as a function of the potential applied to the n^+ points (V_{n+}) for the illuminated Si photoelectrode. (a) $Si/CH_3OH-1.0$ M $LiClO_4-103$ mM Me_2Fc-12 mM Me_2FcBF_4 ($E(A/A^-) = 170$ mV vs SCE), (b) Si/75% THF−25% CH_3OH (v/v)−1.0 M $LiClO_4-4.3 \pm 0.5$ mM Me_{10}-$Fc-4.4 \pm 0.5$ mM $Me_{10}FcBF_4$ ($E(A/A^-) = -23$ mV vs SCE), (c) Si/$CH_3OH-1.0$ M LiCl-10 mM $MV^{+}-21$ mM $MVCl_2$ ($E(A/A^-) = -446$ mV vs SCE), (d) $Si/CH_3OH-0.90$ M $LiCl-2.3 \pm 0.2$ mM $CoCp_2-45$ mM $CoCp_2Cl$ ($E(A/A^-) = -890$ mV vs SCE).

the J_{p+} vs V_{p+} as well as $V_{n+,oc}$ vs V_{p+} relationships under illumination for redox couples that developed significant photovoltages in this contact configuration. In all of these cases, in the potential range where the photocurrent was dependent upon the applied potential, the value of $-V_{n+,oc}$ increased as the forward bias, V_{p+}, decreased. In the region where J_{p+} was

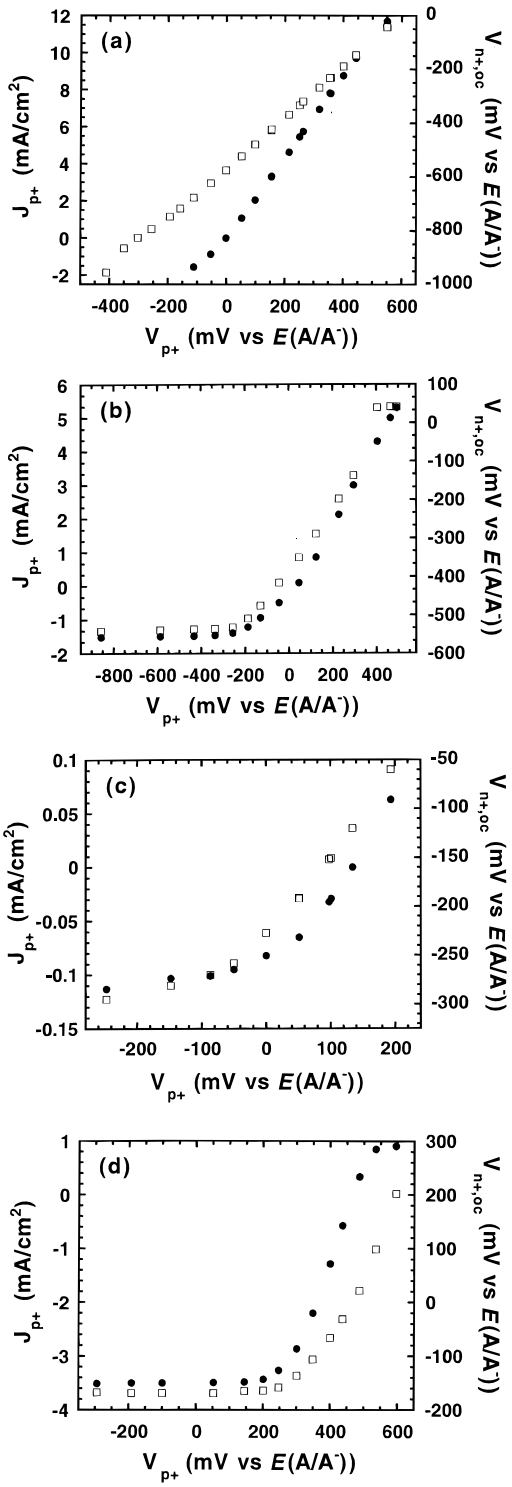

Figure 4. Plot of the open-circuit potential measured at n^+ points ($V_{n+,oc}$, open squares) and current collected at p^+ points (J_{p+}, solid circles) as a function of the potential applied to the n^+ points (V_{p+}) for the illuminated Si photoelectrode. (a) Si/CH_3OH−1.0 M $LiClO_4$−103 mM Me_2Fc−12 mM Me_2FcBF_4 (E(A/A$^-$) = 170 mV vs SCE), (b) Si/80% THF−20% CH_3OH (v/v)−0.54 M $LiClO_4$−23 mM $Me_{10}Fc$−14 mM $Me_{10}FcBF_4$ (E(A/A$^-$) = −3 mV vs SCE), (c) Si/CH_3OH−1.0 M LiCl−6.0 mM MV^+−26 mM $MVCl_2$ (E(A/A$^-$) = −420 mV vs SCE), (d) Si/CH_3OH−0.90 M LiCl−2.3 ± 0.2 mM $CoCp_2$−45 mM $CoCp_2$-Cl (E(A/A$^-$) = −890 mV vs SCE).

independent of V_{p+}, $V_{n+,oc}$ was essentially insensitive to changes in V_{p+}. Thus, in all respects, the behavior observed when holes were controlled potentiostatically corresponds to the observations made when the electrons were controlled potentiostatically (i.e., Figure 4b−d is analogous to Figure 3a−c).

B. Qualitative Understanding of the Experimental Quasi-Fermi Level Behavior under Applied Bias. The data described above show that the potential of the quasi-Fermi level of the carrier type not under potential control was a function of the current density of the carrier being collected through the back of the sample at the regions under potential control. This was true regardless of the energetic position of the electrochemical potential of the solution relative to the valence or conduction band edge energies, and regardless of the carrier type being collected at the back of the sample. Such data are especially important with respect to understanding the behavior of quasi-Fermi levels of illuminated semiconductor photoelectrodes as originally predicted by Gerischer[4] and as discussed extensively in several recent, elegant publications by Memming and co-workers.[5−7,20]

The behavior of the Si/CH_3OH−$Me_2Fc^{+/0}$ junctions with control of the n^+ points (Figure 3a) is readily understood. If collection of electrons at the n^+ contacts results in holes being collected at the solid/liquid interface, changes in V_{n+} should produce changes in the value of $V_{p+,oc}$. Specifically, as the hole flux increases across the solid/liquid contact, $V_{p+,oc}$ should increase to accommodate this increase in interfacial charge transfer. This is exactly the behavior observed experimentally for the Si/CH_3OH−$Me_2Fc^{+/0}$ contact. When the light-limited photocurrent density was reached in this system, the hole flux became constant with changes in the applied potential, and further increases in V_{n+} had no effect on the value of $V_{p+,oc}$. This is also in accord with theoretical expectations, since no further polarization of the hole quasi-Fermi level is required when the interfacial hole flux is constant with variations in potential.

An additional implication of this correlation between the electron and hole fluxes is that the potential necessary to produce a certain interfacial hole flux, measured as the J_{p+} vs V_{p+} relationship for this solid/liquid junction, should be related directly to the J_{n+} vs V_{n+} relationship of this contact. If removal of an electron at the back n^+ contact indeed produces injection of a hole from the valence band into the electrolyte, then the constraint $J_{n+} = -J_{p,f}$ (where $J_{p,f}$ is the interfacial hole current density at the solid/liquid interface) must apply. In other words, if establishing a certain current density of electrons at the back contact (J_{n+}) requires establishing an equal current density (of opposite sign) for holes across the front contact ($J_{p,f}$), then the hole quasi-Fermi level ($V_{p+,oc}$) must move positively at the solid/liquid contact in order to accommodate this specific interfacial hole flux.

This prediction is experimentally testable, because the relationship between the hole quasi-Fermi level and the interfacial hole flux can be experimentally determined from the behavior of J_{p+} vs V_{p+}. If the constraint $J_{n+} = -J_{p,f}$ holds, then a plot of J_{p+} (established by controlling V_{p+}) vs the value of $V_{n+,oc}$ developed for that interfacial hole flux should map onto a plot of J_{n+} vs V_{n+}. As shown in Figure 5a, this is in excellent accord with the experimental data for the Si/CH_3OH−$Me_2Fc^{+/0}$ contact. Thus, for this system, holes obey the same interfacial current density vs quasi-Fermi level relationship regardless of whether their interfacial flux is dictated by biasing their potential directly at the back p^+ points (as "majority carriers") to produce an interfacial hole current at the solid/liquid contact or whether their interfacial flux is the "minority carrier" response to removal of the potentiostatically controlled "majority carrier" at the back contact through biasing the n^+ points and collecting electrons at the back contact. This relationship, which has been experimentally verified for the contacts studied herein, is essentially the underlying, enabling assumption in the quasi-Fermi level description of semiconductor electrochemistry.[4]

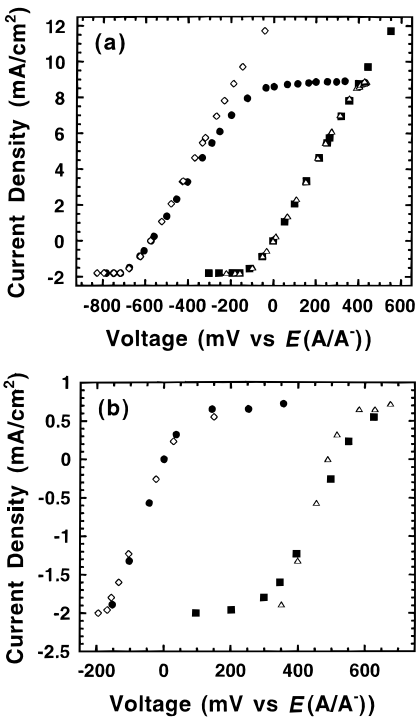

Figure 5. (a) Comparison of the interfacial current density vs quasi-Fermi level relationships for the illuminated Si/CH_3OH−1.0 M $LiClO_4$−103 mM Me_2Fc−12 mM Me_2FcBF_4 (E(A/A^-) = 170 mV vs SCE) contact. The solid circles depict the J_{n+} vs V_{n+} behavior while the open diamonds illustrate the relationship between a given interfacial hole flux, J_{p+}, (established by controlling V_{p+}), and the open-circuit potential developed at the n^+ points, $V_{n+,oc}$. Similarly, the solid squares represent the J_{p+} vs V_{p+} data while the open triangles show the J_{n+} vs $V_{p+,oc}$ relationship. (b) Plot analogous to (a) for the Si/CH_3OH−0.90 M LiCl−14 mM $CoCp_2$−8.0 mM $CoCp_2Cl$ (E(A/A^-) = −915 mV vs SCE) contact. The symbols have the same meaning as in (a).

The same principles can also be applied to the behavior of Si/CH_3OH−$CoCp_2^{+/0}$ junctions. When the p^+ points are controlled potentiostatically, electron transfer with the conduction band dominates the interfacial current flow as discussed above. Thus, collection of holes at the back of the Si (J_{p+}), resulting from biasing the p^+ contact (V_{p+}), requires interfacial electron transfer ($J_{n,f}$) and therefore affects the electron quasi-Fermi level at the solid/liquid contact, in accord with the experimental observations (Figure 4d). As was the case for holes at Si/CH_3OH−$Me_2Fc^{+/0}$ contacts, it was possible to independently determine the relationship between the electron quasi-Fermi level position and the interfacial electron flux (Figure 3d). Applying the constraint that $J_{n,f} = -J_{p+}$, a plot of J_{n+} (established by controlling V_{n+}) vs the value of $V_{p+,oc}$ developed for that interfacial electron flux should map onto a plot of J_{p+} vs V_{p+}. Figure 5b shows that this relationship is also borne out experimentally. Although not shown in the figures of this paper, analogous results were also observed for the redox couples having energies in the middle of the semiconductor bandgap, $MV^{2+/+}$ and $Me_{10}Fc^{+/0}$.

One potentially confounding variable in these measurements is the degree to which the observed values of the quasi-Fermi levels at the back contact ($qV_{n+,oc}$, $qV_{p+,oc}$) reflect the positions of the quasi-Fermi levels at the solid/liquid interface. Since it can be shown both experimentally (see following paper, part 3) and through digital simulation methods of the steady-state response (vide infra) that the potentials measured at the back of the sample are within <2 meV of those at the semiconductor/liquid contact under the experimental conditions used herein, we conclude that the data of Figures 3 and 4 yield direct measurements of the behavior of the quasi-Fermi levels at these semiconductor/liquid junctions.

C. Digital Simulation of the Quasi-Fermi Level Behavior of Si/Liquid Contacts under Applied Bias. *1. Simulations of the Quasi-Fermi Level Behavior of Si/CH_3OH−$Me_2Fc^{+/0}$ Contacts.* A more complete, quantitative understanding of the data presented in section III.A can be obtained by reference to the steady-state quasi-Fermi level profiles computed using a digital simulation of the solid/liquid junction. The ToSCA program provided an opportunity to perform a detailed simulation of the carrier generation, recombination, and transport processes in these samples, while incorporating constraints due to Poisson's equation along with boundary conditions that were appropriate for the back and front surfaces of the Si photoelectrodes studied experimentally in this work. Since the simulation program produced steady-state potential and carrier concentration profiles as a function of distance from the solid/liquid interface (Figure 1a−c), it was used to confirm the qualitative arguments advanced above regarding the behavior of the quasi-Fermi levels under various combinations of applied bias and redox potential conditions. In addition, the simulations yielded insight into the behavior of the quasi-Fermi levels under strong reverse bias that were observed experimentally and into other aspects of the $J-V$ data that have not been addressed in the preceding analysis.

Simulations were carried out for Si/$Me_2Fc^{+/0}$, Si/$MV^{2+/+}$, and Si/$CoCp_2^{+/0}$ solid/liquid contacts. The input photon intensity (i.e., the steady-state charge carrier generation rate) was chosen to produce good agreement between the simulated and experimentally measured steady-state current densities (3.5 mA cm^{-2}) and open-circuit voltages. Simulations were performed for a series of applied voltages ranging from forward biases larger than $|V_{oc}|$ to voltages well into reverse bias. At each potential, the carrier concentrations, semiconductor band edge energies, and quasi-Fermi levels were computed as a function of position in the semiconductor.

Figure 6a depicts the computed J_{n+} vs V_{n+} behavior of the Si/CH_3OH−$Me_2Fc^{+/0}$ contact along with the computed $V_{p+,oc}$ vs V_{n+} relationship of this system. This simulation represented a limiting case in which **E**(A/A^-) was close to one of the band edge positions. (**E**(A/A^-) is near $\mathbf{E}_v$ in this particular situation.) The simulations were able to reproduce the general form of the experimental data. At the open-circuit potential ($V_{n+} \approx -0.6$ V), $V_{p+,oc}$ is calculated to be 0 V, in accord with experimental observations. As V_{n+} moved positively from $V_{n+,oc}$ toward reverse bias, the current density increased until it reached a plateau in which J_{n+} was limited by the photogenerated carrier flux. For this same potential regime, the simulations showed that the hole concentration at the electrode surface, and thus the interfacial hole flux into the solution ($J_{p,f}$), increased as J_{n+} increased. In this region of control over V_{n+}, the value of $V_{p+,oc}$ increased only slightly (3 mV) in the simulation relative to its value at open circuit (0 V vs the Nernstian potential of the cell, E(A/A^-)). In further reverse bias, the computed J_{n+} was independent of V_{n+}, and the computed $V_{p+,oc}$ also became independent of V_{n+}. The lack of change in $V_{p+,oc}$ when J_{n+} is constant is in accord with the experimental data. However, the experimental $V_{p+,oc}$ value for the Si/CH_3OH−$Me_2Fc^{+/0}$ contact increased monotonically with increasing reverse bias until reaching a value of ≈0.4 V vs E(A/A^-) (Figure 3a). The difference between the simulated and observed plateau values of $V_{p+,oc}$ is readily explained by the lack of incorporation into the simulation routine of concentration polarization and series resistance losses in the solution, whereas the actual photoelectrochemical cell must experience these overpotentials

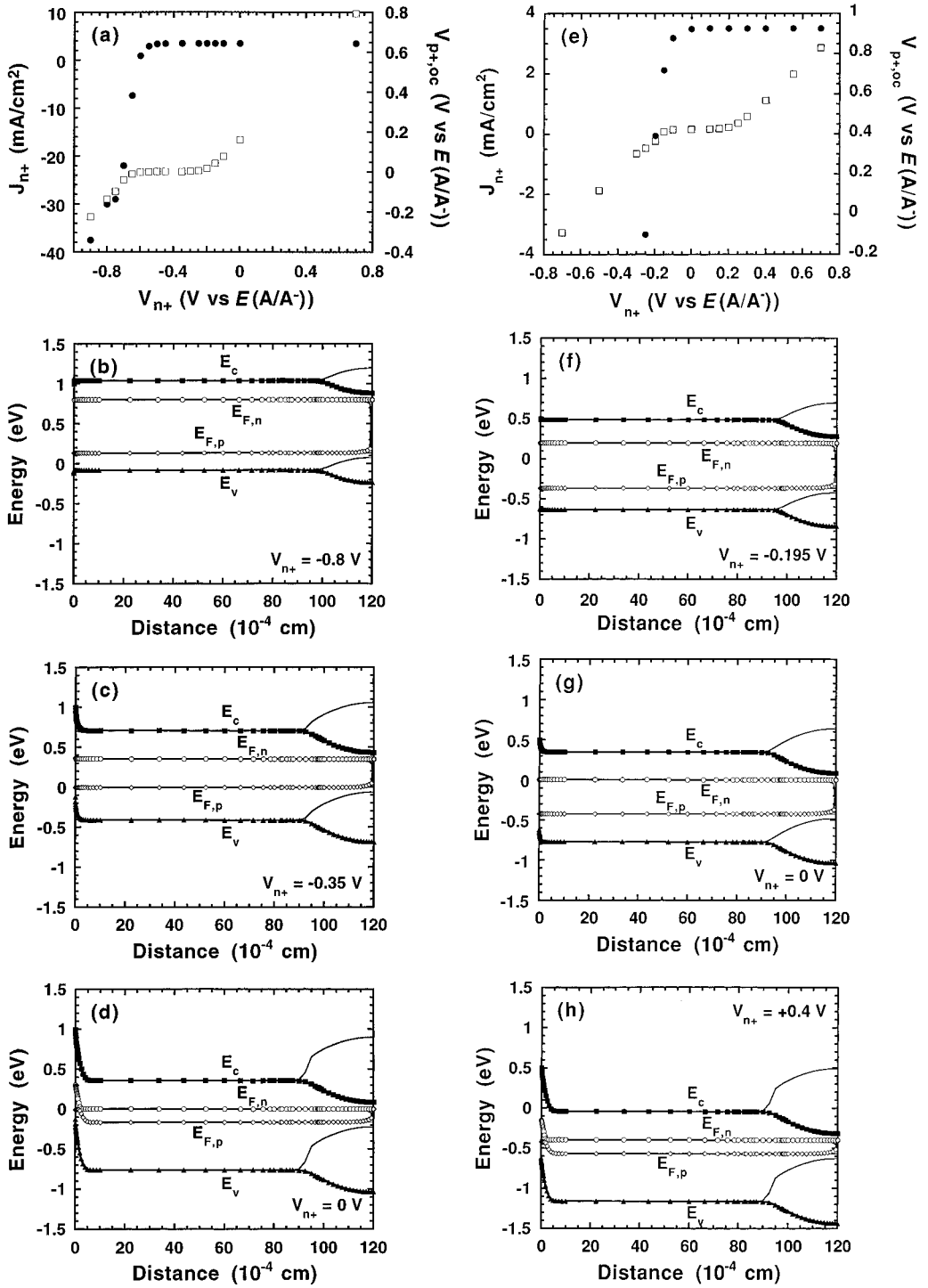

Figure 6. Results of 2-dimensional computer simulations for illuminated n-Si/$Me_2Fc^{+/0}$ (a−d) and n-Si/$MV^{2+/+}$ systems (e−h). (a) The current density−voltage curve for the $Me_2Fc^{+/0}$ contact (solid circles) is shown along with the calculated open-circuit voltages at the p^+ points when the potential is applied to the n^+ points (open squares). The rate constants for the electron and hole transfer were assumed to be equal, with $k_{ct}^{max} = 10^{-18}$ cm^4 s^{-1}. The concentrations were $c_{red} = 110$ mM and $c_{ox} = 16$ mM, and the barrier height of the contact was 1.0 V.[25,30−35] (b−d) Profiles of the quasi-Fermi levels (open circle depict $\mathbf{E}_{F,n}$ and open diamonds depict $\mathbf{E}_{F,p}$) and of the conduction and valence band energies (solid squares depict $\mathbf{E}_c$ and solid triangles depict $\mathbf{E}_v$) along a cut perpendicular to the surface and passing through the center of the n^+ points. The solid lines represent a corresponding cut through the center of the p^+ points. (e) The current density−voltage curve for the $MV^{2+/+}$ contact (solid circles) is shown along with the calculated open-circuit voltages at the p^+ points when the potential is applied to the n^+ points (open squares). The rate constants for the electron and hole transfer were assumed to be equal, with $k_{ct}^{max} = 10^{-18}$ cm^4 s^{-1}. The concentrations were $c_{red} = 10$ mM and $c_{ox} = 21$ mM, and the barrier height of the contact was 0.5 V.[36] (f−h) Profiles of the quasi-Fermi levels and of the conduction and valence bands along a cut perpendicular to the surface and passing through the center of the n^+ points. The symbols have the same meaning as in (b−d), and the solid lines represent a corresponding cut through the center of the p^+ points.

in order to sustain a net interfacial current flow. The self-consistency between the independently measured concentration polarization/series resistance losses for holes evident in the J_{p+} vs V_{p+} plots and those reflected in the $V_{p+,oc}$ vs V_{n+} behavior (Figure 3a) clearly indicates that these factors are responsible for the difference between the simulated behavior and the experimental data.

Figure 6b,c displays the quasi-Fermi level profiles of electrons and holes and the electric potential profiles vs distance that were computed for representative values of V_{n+} in each of these

regions of $V_{p+,oc}$ vs V_{n+} behavior. These profiles represent two sections through the semiconductor, both of which are perpendicular to the surface and pass through the center of the n^+ or p^+ contacts. In both cases, the simulations verified that the quasi-Fermi levels were essentially flat across the sample, so the values at the edges of the point contacts provided reliable estimates of the values of the quasi-Fermi levels at the solid/liquid interface. The simulations also verified the qualitative relationships discussed above between $V_{p+,oc}$ and V_{n+}. In essence, the value of n_s was set by the potentiostatically controlled value of V_{n+}, and the hole concentration at the electrode surface adjusted so that the condition $J_{p,f} = -J_{n+}$ was met. In this fashion, changes in V_{n+} for the Si/$CH_3OH-Me_2Fc^{+/0}$ contact effected changes in $V_{p+,oc}$ through the constraint that $J_{p,f} = -J_{n+}$, thereby linking the electron and hole quasi-Fermi levels and producing simulated electrode behavior in excellent accord with the experimental data.

The simulation of the Si/$CH_3OH-Me_2Fc^{+/0}$ contact also addressed another aspect of the $V_{p+,oc}$ vs V_{n+} properties in that it predicted a third region of $V_{p+,oc}$ vs V_{n+} behavior. As mentioned earlier, the experimental value of $V_{p+,oc}$ became linearly dependent on V_{n+} at large positive V_{n+} values. This is an interesting result because J_{n+} is constant in this region, so the interfacial hole flux should have remained constant as V_{n+} varied. The experimental behavior was indeed obtained from the digital simulation results. There are two possible reasons for such $V_{p+,oc}$ vs V_{n+} behavior: (a) as V_{n+} is increased, a shift in the band edges occurs as excess holes are built up at the solid/liquid interface, producing a voltage drop that would be reflected in the value of $V_{p+,oc}$ measured at the back surface of the semiconductor, and/or (b) the quasi-Fermi levels are no longer flat across the sample so that a change in $V_{p+,oc}$ does not necessarily correspond to a change in the surface concentration of holes (dictating $J_{p,f}$). The digital simulation clearly showed that the quasi-Fermi levels are no longer constant across the sample at large reverse biases (Figure 6d). Additionally, neither a significant change in the band edge position at the solid/liquid interface nor a significant increase in the hole concentration at the semiconductor surface was computed in the simulation. Thus, this third region of $V_{p+,oc}$ vs V_{n+} behavior is evidently an inherent feature of the samples and did not require an excess charge buildup or slow interfacial kinetics to produce a large voltage drop across the Helmholtz layer. This aspect of the $V_{p+,oc}$ vs V_{n+} behavior required the detailed digital simulation to be evaluated quantitatively.

2. Simulations of the Quasi-Fermi Level Behavior of Si/$CH_3OH-MV^{2+/+}$ Contacts. Digital simulations were also performed on a representative Si/liquid contact for which the electrochemical potential of the solution was located near the middle of the Si band gap. Figure 6e shows the calculated J_{n+} vs V_{n+} behavior along with the $V_{p+,oc}$ vs V_{n+} data for the Si/$CH_3OH-MV^{2+/+}$ system. In Figure 6f−h, the quasi-Fermi level profiles and electric potential profiles along lines perpendicular to the surface and through the centers of the two selective ohmic back contacts are displayed for representative V_{n+} values of this junction. The computed behavior was similar to that of the Si/$CH_3OH-Me_2Fc^{+/0}$ system but displayed a few significant differences. First, when the n^+ points were at their open-circuit potential, the computed quasi-Fermi level for holes was not equal to the Nernstian potential of the solution ($V_{p+,oc} \neq 0$) (Figure 6e). This behavior is in accord with the experimental observations (Figure 3c above and Figure 4 in the preceding paper) and indicates that the surface concentration of holes required to reach open circuit at the specified light intensity is larger than the equilibrium hole concentration at the surface ($p_s/p_{so} > 1$). This is in contrast to the situation for redox couples having **E**(A/A^-) close to one band edge, in which the current is almost completely due to the transfer of one carrier type.

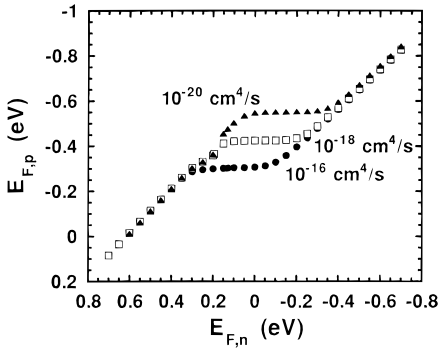

Figure 7. Results of one-dimensional computer simulations for the n-Si/$MV^{2+/+}$ system demonstrating the dependence of the quasi-Fermi level of holes (open circuit potential at the p^+ points) on the quasi-Fermi level of electrons (potential is applied at the n^+ points) for three different charge-transfer rate constants, k_{ct}^{max} (filled circles, 10^{-16} cm^4 s^{-1}; open squares, 10^{-18} cm^4 s^{-1}; filled triangles, 10^{-20} cm^4 s^{-1}). In each case the rate constants for the electron and hole transfer were assumed to be equal (k_{ct}^{max}). The concentrations were $c_{ox} = 21$ mM and $c_{red} = 10$ mM, and the barrier height of the contact was $\Phi_b = 0.5$ eV.[36]

A second difference between the simulated behavior of the Si/$CH_3OH-MV^{2+/+}$ and Si/$CH_3OH-Me_2Fc^{+/0}$ contacts was the delayed onset of the region at reverse bias in which $V_{p+,oc}$ increased with more positive values of V_{n+}. This change in the $V_{p+,oc}$ vs V_{n+} behavior occurred despite no change in the light-limited value of J_{n+} over this range of V_{n+} values. As shown in Figure 7, the simulations revealed that the value of V_{n+} at which this behavior occurred depended strongly on the value of the interfacial hole transfer rate constant in the system. This behavior is readily understood by reference to the quasi-Fermi level profiles depicted in Figure 6f−h. Relatively large interfacial charge-transfer rate constants required relatively low hole concentrations at the electrode surface to produce the desired interfacial hole flux. Thus, for large k_v^{max} values, the value of $V_{p+,oc}$ did not deviate greatly from its equilibrium value for moderate values of V_{n+}. However, further increases in V_{n+} resulted in the quasi-Fermi levels varying across the semiconductor sample, and this produced significant changes in $V_{p+,oc}$. In contrast, small k_v^{max} values required a significant increase in the concentration of holes at the surface as well as in the bulk and thus (i) extended the range over which the $V_{p+,oc}$ increased with more positive V_{n+} values and (ii) increased the value of $V_{p+,oc}$ in the plateau region, indicating that the surface concentration of holes is larger under such conditions than would be required with larger values of k_v^{max}.

3. *Simulations of the Quasi-Fermi Level Behavior of Si/$CH_3OH-CoCp_2^{+/0}$ Contacts.* An analogous set of simulations was performed for Si/$CH_3OH-CoCp_2^{+/0}$ contacts. For this system, the J_{p+} vs V_{p+} behavior under illumination was modeled along with the V_{p+} vs $V_{n+,oc}$ relationship (not shown). In almost all aspects, the simulated plots exhibited features that were analogous to those computed for Si/$CH_3OH-Me_2Fc^{+/0}$ contacts, except that the currents were of opposite sign. In the region where the photocurrent was dependent on the applied potential, the value of $V_{n+,oc}$ was calculated to be linearly dependent on V_{p+}. In the region where the photocurrent was constant with potential, no further increase in the surface electron concentration was required to fulfill the constraint $J_{n,f} = J_{p+}$, and therefore, no further negative shift in $V_{n+,oc}$ was calculated until the value of the V_{p+} was negative enough that the quasi-Fermi levels started to bend near the surface.

The digital simulations also reproduced the experimentally observed behavior that, at a constant light intensity, the quasi-Fermi level separation, $qV_{p+,oc} - qV_{n+,oc}$, was greatest for systems having a redox potential near either the conduction band edge or valence band edge. Smaller $V_{p+,oc} - V_{n+,oc}$ values, and therefore more total recombination, were observed for the two redox couples having $\mathbf{E}(A/A^-)$ nearer the middle of the semiconductor band gap (see preceding paper). The computer simulations also showed that the energy bands were flat at V_{oc} for redox couples having electrochemical potentials near the middle of the band gap. On the other hand, if the electrochemical potential of the solution is close to one of the energy band edges, the simulations showed a residual electrical field at V_{oc} even under the high level injection conditions applied in the experiments.

4. The Quasi-Fermi Level Behavior of Systems Exhibiting Nonrectifying J−V Behavior under Illumination. The quasi-Fermi level behavior observed at the n^+ points during potentiostatic control over the p^+ potential at $Si/CH_3OH-Me_2Fc^{+/0}$ interfaces (Figure 4a), and at the p^+ points during potentiostatic control of the n^+ points for $Si/CH_3OH-CoCp_2^{+/0}$ contacts (Figure 3d), was also revealed by the digital simulations. Hole transfer with the valence band has already been identified as the dominant interfacial current flow at the $Si/CH_3OH-Me_2Fc^{+/0}$ contact.[53,54] Thus, removing an electron from the back of these intrinsic Si samples results in hole transfer into the solution at this solid/liquid interface. Nevertheless, when holes are removed at the back p^+ contact, the value of the electron quasi-Fermi level was observed to shift, even though holes, not electrons, were injected across the solid/liquid contact. The digital simulation revealed that this unexpected behavior arose because, under these specific circumstances, the quasi-Fermi levels were not flat across the sample. Instead, the measured value of V_{n+} at the back of the sample did not accurately reflect the potential corresponding to the electron quasi-Fermi level position at the solid/liquid contact. Thus, the dependence of $V_{n+,oc}$ on the value of V_{p+} is a consequence of the experimental contact geometry in the sample and does not imply that manipulation of the hole concentration at the p^+ points produced interfacial electron transfer or a change in the value of the electron quasi-Fermi level at the $Si/CH_3OH-Me_2Fc^{+/0}$ contact.

The behavior observed at the p^+ points during potentiostatic control of the n^+ points for the $Si/CH_3OH-CoCp_2^{+/0}$ system was analogous to that seen in the reverse contact configuration for the $Si/CH_3OH-Me_2Fc^{+/0}$ contact. The hole quasi-Fermi level position was affected by changes in bias at the n^+ points even though the interfacial current in this system is completely dominated by electron transfer with the conduction band. While this behavior is similar to that observed for $Si/CH_3OH-Me_2Fc^{+/0}$ interfaces, digital simulations revealed the underlying physical phenomena to be different. For the $Si/CH_3OH-CoCp_2^{+/0}$ system, the quasi-Fermi levels were calculated to remain flat across the sample, but a monotonic shift was predicted to occur in the band edge positions as a function of the applied potential. This information was both interesting and satisfying because such shifts in V_{n+} as V_{p+} was varied were unexpected but were correctly accounted for by the simulation package. This agreement between experiment and simulation provided confidence that the properties of the semiconductor/liquid contact were being accounted for correctly by the simulation routine.

5. Correlations between the Back Contact Fluxes and Fluxes at the Semiconductor/Liquid Junction. The simulations for the systems having $\mathbf{E}(A/A^-)$ close to one of the energy band edges of the semiconductor are summarized in Figure 8. The results

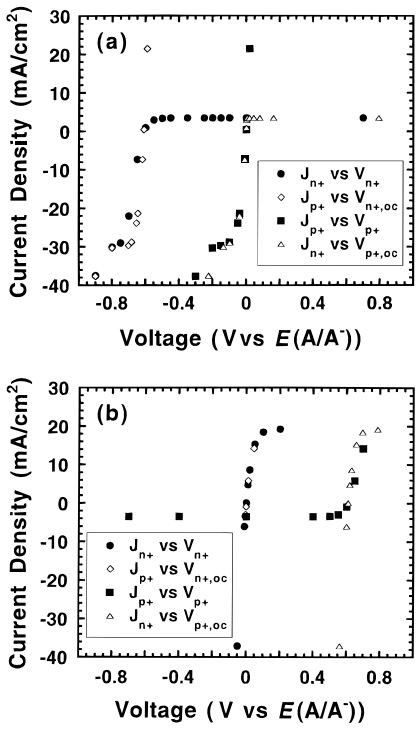

Figure 8. (a) Results of two-dimensional computer simulations for the n-$Si/Me_2Fc^{+/0}$ system: comparison of the interfacial current density vs quasi-Fermi level relationships. The rate constants for the electron and hole transfer were assumed to be equal with $k_{ct}^{max} = 10^{-18}$ cm^4 s^{-1}. The concentrations were $c_{ox} = 16$ mM and $c_{red} = 110$ mM, and the barrier height of the contact was 1.0 V.[25,30−35] The meanings of the symbols are given in the inset. (b) Plot analogous to (a) for the n-$Si/CoCp_2^{+/0}$ system. The rate constants for the electron and hole transfer were assumed to be equal, with $k_{ct}^{max} = 10^{-18}$ cm^4 s^{-1}. The concentrations were $c_{red} = 2$ mM and $c_{ox} = 45$ mM, and the energy difference between the conduction band and the electrochemical potential of the solution was taken to be 0.12 eV.[36]

confirm the experimental observations presented in Figure 5. If the overall charge transfer at the solid/liquid interface is dominated by one carrier type (e.g., electron transfer between the $CoCp_2^{+/0}$ redox couple and the silicon conduction band), the potential at the corresponding (n^+) point back contact represents a measure of the concentration of that carrier at the electrode surface and thus is directly related to the current density at the front contact ($|J_{n,f}| \gg J_{p,f}$, eqs 11 and 12 in part 1). The observations and simulations presented herein therefore confirm that the current density of each carrier type at the solid/liquid contact is identical for a given carrier potential, regardless of whether the potential of interest is obtained by applying a bias to the back of the semiconductor, and thus directly influencing the carrier of concern, or whether the other carrier type is controlled potentiostatically, indirectly producing a flux of the probed carrier type at the solid/liquid contact.

Our results are fully consistent with the quasi-Fermi level concept that has been used by Memming and co-workers previously to describe processes in semiconductor photoelectrochemistry.[5,6,55] In earlier work, a comparison between reaction rates at n-type and p-type electrodes was required in order to investigate experimentally the applicability of the quasi-Fermi level concept. In the present study, the use of high purity, low dopant density Si electrodes with ohmic selective back contacts has allowed the direct measurement of the quasi-Fermi levels individually and simultaneously for a single semiconductor/liquid junction. This feature has allowed us to explore several aspects of quasi-Fermi level behavior that have not been probed previously. In general, the results described herein have validated the basic applications of the quasi-Fermi level

concepts, at open circuit and under applied bias conditions, for both carrier types, in these Si/CH_3OH junction photoelectrochemical cells.

IV. Summary

In this study, the quasi-Fermi levels were probed experimentally and exhibited behavior that was consistent with the predictions of the basic model for semiconductor electrochemistry. The current density−voltage behavior of a specific charge carrier in these samples was observed to be the same regardless of whether it was a "majority" carrier, whose flux was specified by an applied potential at the back of the sample, or a "minority" carrier, whose interfacial flux was generated by optical absorption of bandgap illumination in the photostationary state of a biased semiconductor/liquid contact. The general behavior of these quasi-Fermi levels can be understood based on simple principles, but certain aspects required a detailed analysis of the generation, recombination, and transport properties of the specific sample geometry of concern. Digital simulations provided by the ToSCA package were in excellent accord with all of the essential aspects of the experimental behavior. These nearly intrinsic photoelectrodes, operated under high level injection, thus offer a unique opportunity to investigate the behavior of kinetically controlled charge separation processes in a semiconductor photoelectrode. They also have provided previously unavailable experimental insight into the behavior of quasi-Fermi levels at illuminated semiconductor/liquid contacts. Such information is relevant to the behavior of particulate photoelectrochemical systems, to intrinsic photoelectrode behavior, and to a variety of other aspects of semiconductor photoelectrochemistry. The experimental behavior and digital simulations described herein (and the time-dependent behavior described in part 3) provide a relatively complete picture of the photoelectrochemical properties of such systems and serve to advance, both qualitatively and quantitatively, the analytical description of charge separation and collection events at illuminated semiconductor/liquid contacts.

Acknowledgment. We acknowledge the National Science Foundation, Grant CHE-9634152, for support of this research. O.K. acknowledges the Deutsche Forschungsgemeinschaft for a postdoctoral fellowship, and M.X.T. acknowledges the Link Foundation and W.R. Grace, Inc., for graduate fellowships. We also thank Prof. H. Gajewski and Dr. R. Nürnberg for their support and valuable help during the modification and application of the ToSCA program package.

References and Notes

(1) Tan, M. X.; Kenyon, C. N.; Krüger, O.; Lewis, N. S. *J. Phys. Chem.* **1997**, *101*, 2830.
(2) Nozik, A. J. *Annu. Rev. Phys. Chem.* **1978**, *29*, 189.
(3) Williams, F.; Nozik, A. J. *Nature* **1978**, *271*, 137.
(4) Gerischer, H. In *Solar Energy Conversion. Solid-State Physics Aspects*; Seraphin, B. O., Ed.; Springer-Verlag: Berlin, 1979; Vol. 31, p 115.
(5) Reineke, R.; Memming, R. *J. Phys. Chem.* **1992**, *96*, 1310.
(6) Reineke, R.; Memming, R. *J. Phys. Chem.* **1992**, *96*, 1317.
(7) Meissner, D.; Memming, R. *Electrochim. Acta* **1992**, *37*, 799.
(8) Gregg, B. A.; Nozik, A. J. *J. Phys. Chem.* **1993**, *97*, 13441.
(9) Shreve, G. A.; Lewis, N. S. *J. Electrochem. Soc.* **1995**, *142*, 112.
(10) Tan, M. X.; Kenyon, C. N.; Lewis, N. S. *J. Phys. Chem.* **1994**, *98*, 4959.
(11) Tan, M. X.; Kenyon, C. N.; Wilisch, W. C. A.; Lewis, N. S. *J. Electrochem. Soc.* **1995**, *142*, L62.
(12) Kenyon, C. N.; Tan, M. X.; Krüger, O.; Lewis, N. S. *J. Phys. Chem.* **1997**, *101*, 2850.
(13) Gajewski, H. *GAMM (Ges. Angew. Math. Mech.) Mitteilungen* **1993**, *16*, 35.
(14) van Roosbroeck, W. *Bell Syst. Technol. J.* **1950**, *29*, 560.
(15) Krüger, O.; Jung, C.; Gajewski, H. *J. Phys. Chem.* **1994**, *98*, 12653.
(16) Forker, W. *Elektrochemische Kinetik*; Akademie-Verlag: Berlin, 1989; p 35.
(17) Marcus, R. A. *Annu. Rev. Phys. Chem.* **1964**, *15*, 155.
(18) Gerischer, H. In *Physical Chemistry: An Advanced Treatise*; Eyring, H., Henderson, D., Yost, W., Eds.; Academic: New York, 1970; Vol. 9A, p 463.
(19) Kumar, A.; Wilisch, W. C. A.; Lewis, N. S. *CRC Crit. Rev.* **1993**, *18*, 327.
(20) Memming, R. In *Electron-Transfer I*; Mattay, J., Ed.; Springer-Verlag: Berlin, 1994; Vol. 169, p 105.
(21) Tan, M. X.; Laibinis, P. E.; Nguyen, S. T.; Kesselman, J. M.; Stanton, C. E.; Lewis, N. S. *Prog. Inorg. Chem.* **1994**, *41*, 21.
(22) The normalization factor, $(4\pi\lambda kT)^{-1/2}$, for the distribution of energy states in a redox system is included in the quoted charge-transfer rate constants, as specified in ref 20.
(23) Lewis, N. S. *Annu. Rev. Phys. Chem.* **1991**, *42*, 543.
(24) Koval, C. A.; Howard, J. N. *Chem. Rev. (Washington, D.C.)* **1992**, *92*, 411.
(25) Pomykal, K. E.; Fajardo, A. M.; Lewis, N. S. *J. Phys. Chem.* **1996**, *100*, 3652.
(26) Gerischer, H. *Z. Phys. Chem. (Munich)* **1960**, *26*, 223.
(27) Memming, R. In *Electroanalytical Chemistry*; Bard, A. J., Ed.; Marcel Dekker: New York, 1979; Vol. 11, p 1.
(28) Morrison, S. R. *Electrochemistry at Semiconductor and Oxidized Metal Electrodes*; Plenum Press: New York, 1980.
(29) Williams, F.; Nozik, A. J. *Nature* **1984**, *312*, 21.
(30) Tomkiewicz, M. *Electrochim. Acta* **1990**, *35*, 1631.
(31) Kobayashi, H.; Chigami, A.; Takeda, N.; Tsubomura, H. *J. Electroanal. Chem.* **1990**, *287*, 239.
(32) Kobayashi, H.; Takeda, N.; Sugahara, H.; Tsubomura, H. *J. Phys. Chem.* **1991**, *95*, 813.
(33) Kobayashi, H.; Ono, J.; Ishida, T.; Okamoto, M.; Kawanaka, H.; Tsubomura, H. *J. Electroanal. Chem.* **1991**, *312*, 57.
(34) Laibinis, P. E.; Stanton, C. E.; Lewis, N. S. *J. Phys. Chem.* **1994**, *98*, 8765.
(35) Pomykal, K. E.; Fajardo, A. M.; Lewis, N. S. *J. Phys. Chem.* **1995**, *99*, 8302.
(36) Fajardo, A. M.; Lewis, N. S. *Science* **1996**, *274*, 969.
(37) Marcus, R. A. *J. Phys. Chem.* **1963**, *67*, 853.
(38) Howard, J. N.; Koval, C. A. *Anal. Chem.* **1994**, *66*, 4525.
(39) Watts, D. K.; Koval, C. A. *J. Phys. Chem.* **1996**, *100*, 5509.
(40) Marcus, R. A. *J. Chem. Phys.* **1965**, *43*, 679.
(41) Marcus, R. A. *J. Phys. Chem.* **1990**, *94*, 1050.
(42) Smith, B. B.; Koval, C. A. *J. Electroanal. Chem.* **1990**, *277*, 43.
(43) Yang, E. S.; Chan, M.; Wahl, A. C. *J. Phys. Chem.* **1975**, *79*, 2049.
(44) Bock, C. R.; Connor, J. A.; Gutierrez, A. R.; Meyer, T. J.; Whitten, D. G.; Sullivan, B. P.; Nagle, J. K. *Chem. Phys. Lett.* **1979**, *61*, 522.
(45) Yang, E. S.; Chan, M. S.; Wahl, A. C. *J. Phys. Chem.* **1980**, *84*, 3094.
(46) Nielson, R. M.; McManis, G., E.; Golovin, M. N.; Weaver, M. J. *J. Phys. Chem.* **1988**, *92*, 3441.
(47) Nielson, R. M.; McManis, G. E.; Safford, L. K.; Weaver, M. J. *J. Phys. Chem.* **1989**, *93*, 2152.
(48) McManis, G. E.; Nielson, R. M.; Gochev, A.; Weaver, M. J. *J. Am. Chem. Soc.* **1989**, *111*, 5533.
(49) Sinton, R. A.; Kwark, Y.; Gan, J. Y.; Swanson, R. M. *IEEE Electron Device Lett.* **1986**, *EDL-7*, 567.
(50) Forbes, M. D. E.; Lewis, N. S. *J. Am. Chem. Soc.* **1990**, *112*, 3682.
(51) Fajardo, A. M.; Karp, C. D.; Kenyon, C. N.; Pomykal, K. E.; Shreve, G. A.; Tan, M. X.; Lewis, N. S. *Sol. Energy Mater. Sol. Cells* **1995**, *38*, 279.
(52) Tan, M. X.; Lewis, N. S. *Inorg. Chim. Acta* **1996**, *242*, 311.
(53) Rosenbluth, M. L.; Lieber, C. M.; Lewis, N. S. *Appl. Phys. Lett.* **1984**, *45*, 423.
(54) Rosenbluth, M. L.; Lewis, N. S. *J. Am. Chem. Soc.* **1986**, *108*, 4689.
(55) Reineke, R. Ph.D. Thesis, Hamburg, 1988.
(56) Sze, S. M. *The Physics of Semiconductor Devices*, 2nd ed.; John Wiley and Sons: New York, 1981.
(57) Blinov, L. M.; Bobrova, E. A.; Vavilov, V. S.; Galkin, G. N. *Fiz. Tverd. Tela* **1967**, *9*, 3221.
(58) Nilsson, N. G.; Svantesson, K. G. *Solid State Commun.* **1972**, *11*, 155.
(59) Dziewior, J.; Schmid, W. *Appl. Phys. Lett.* **1977**, *31*, 346.
(60) Fossum, J. G.; Mertens, R. P.; Lee, D. S.; Nijs, J. F. *Solid-State Electron.* **1983**, *26*, 569.
(61) Tyagi, M. S.; Van Overstraeten, R. *Solid-State Electron.* **1983**, *26*, 577.
(62) Internally, ToSCA utilizes the physics convention for the sign of the electric potential (i.e., a positively charged space charge region is a region having more negative potential). This convention is opposite to the IUPAC convention (ref 21) traditionally used in electrochemistry. For consistency, all equations in the present work have been specified using the IUPAC convention.